Multitarget Evaluation of Hybrid Electric Vehicle Powertrain Architectures Considering Fuel Economy and Battery Lifetime

2020-37-0015

Multitarget Evaluation of Hybrid Electric Vehicle Powertrain Architectures considering Fuel Economy and Battery Lifetime

Pier Giuseppe Anselma[1], Phillip Kollmeyer[2], Giovanni Belingardi[1], Ali Emadi[2]
[1]Politecnico di Torino, [2]McMaster University

Abstract

Hybrid electric vehicle (HEV) powertrains are characterized by a complex design environment as a result of both the large number of possible layouts and the need for dedicated energy management strategies. When selecting the most suitable hybrid powertrain architecture at an early design stage of HEVs, engineers usually focus solely on fuel economy (directly linked to tailpipe emissions) and vehicle drivability performance. However, high voltage batteries are a crucial component of HEVs as well in terms of performance and cost. This paper introduces a multitarget assessment framework for HEV powertrain architectures which considers both fuel economy and battery lifetime. A multi-objective formulation of dynamic programming is initially presented as an off-line optimal HEV energy management strategy capable of predicting both fuel economy performance and battery lifetime of HEV powertrain layout options. Subsequently, three different HEV powertrain architectures are considered as test cases for the developed HEV assessment methodology including parallel P2, series-parallel P1P2 and power-split layouts. A comparison of numerical results for the three HEV powertrain test cases is then performed in terms of optimal fuel economy capabilities while ensuring a specific battery lifetime over several defined driving missions. Engineers could thus adopt the developed methodology to enhance the evaluation of HEV design options by considering fuel economy and battery lifetime at the same time.

Introduction

Hybrid electric vehicles (HEVs) represent a promising technology from the perspective of automotive OEMs as they enable compliance with fuel consumption and tailpipe emission regulations over the next few years [1]. On the other hand, designing HEVs is more complicated compared to both battery electric vehicles (BEVs) that are powered by electric motors solely, and conventional vehicles that are powered by internal combustion engines (ICEs) solely [2]. Difficulties in HEV powertrain design and sizing relate both to the number of power components (i.e. one ICE, one or multiple electric motor/generators (MGs), a high-voltage battery, dedicated power electronics) and the necessity of a suitable complementary energy management strategy (EMS) [3]. In general, several different categories of HEV powertrain architectures can be defined including series, parallel, series-parallel, power-split and multimode power-split as an example [4].

When selecting the hybrid powertrain architecture and component sizes at early HEV design stages, numerical simulations are usually performed which consider design candidates controlled by off-line EMSs over pre-selected driving missions. Off-line EMSs utilize future knowledge (i.e. the speed, terrain, and other environmental conditions) of drive cycles of interest to optimize the overall hybrid powertrain operation [5]. Examples of off-line EMSs for HEV powertrains include dynamic programming (DP) [6], Pontryagin's minimum principle (PMP) [7], power-weighted efficiency analysis for rapid sizing (PEARS) [8], slope-weighted energy-based rapid control analysis (SERCA) [9] and convex optimization [10]. Among them, DP is currently the most adopted off-line EMS for HEVs due to its ability to effectively return a global optimal solution for the considered control problem. Moreover, DP algorithms can be quite easily adapted to different HEV powertrain architectures and component sizes [11]. Off-line EMSs for HEVs are usually employed to solve an optimization problem considering fuel economy (FE) solely over retained driving missions [12]. Nevertheless, an urgent need can be identified in accounting for further criteria (e.g. noise vibration harshness, thermal management, after-treatment system) when optimizing the hybrid powertrain operation through off-line EMSs [13].

Among the components of an HEV powertrain, high-voltage batteries are crucial both from operational and cost points of view. A key requirement for the battery is that it must provide the electrical power demanded from electric motor/generators (MGs) over its entire lifetime. Moreover, the battery lifetime (BL) should be guaranteed to equal or exceed the overall vehicle lifetime in favor of overall vehicle ease of maintenance, cost of ownership and limitation in emitted CO_2 due to the production of a replacement battery. Literature about lifetime of high-voltage batteries for HEVs has usually concentrated on empirical ageing tests [14] or on-board estimation of battery ageing effects as example [15]. Moreover, few examples can be found regarding the development of EMSs for HEV powertrains including BL consideration. In 2012, a battery state-of-health perceptive EMS for a P2 HEV powertrain architecture based on the PMP was first presented [16]. A similar study was performed in 2015 for the same HEV powertrain architecture while replacing the automated gearbox with a continuously variable transmission [17]. In 2016, a two-point optimization problem was solved using DP for a plug-in HEV while retaining an application-specific target battery life as the objective of the HEV EMS [18]. A parallel P2 HEV architecture was investigated in 2018 as well, where results for a PMP-based and a DP-based multi-objective EMS considering both

FE and battery ageing were presented [19]. Recently, the effectiveness of convex optimization has been suggested when considering battery state-of-health (SOH) as an additional control target for a plug-in series hybrid electric city bus [20]. Nevertheless, all the mentioned research works considered a single HEV powertrain architecture (usually of parallel P2 type). This paper therefore aims at assessing different full hybrid powertrain architectures considering both FE and BL as optimization targets. A DP formulation is firstly developed that can return a global optimal solution for the operation of the considered HEV powertrain architectures considering a weighted average of FE and BL targets. Then, different HEV powertrain architectures are analyzed considering the proposed DP approach, i.e. parallel, series-parallel and power-split. The remainder of the paper is organized as follows: the analyzed HEV powertrain architectures are firstly illustrated and modeled. Then, the numerical approach adopted to model the high-voltage battery ageing is illustrated. The multi-target HEV off-line control problem considering FE and BL is consequently developed and the performance using the developed DP approach is discussed. Finally, results and conclusions are given.

Hybrid powertrain architectures

The considered hybrid powertrain architectures including parallel, series-parallel and power-split layouts are defined and discussed in this section.

Parallel P2

Among the different hybrid architectures, parallel HEVs have been selected by many car manufacturers as their first step into vehicle electrification [21]. In a parallel HEV, the tractive power is combined: both the ICE and the MGs can contribute to the vehicle propulsion, i.e. their corresponding torques are additive. When the MG is large enough, it can drive the HEV by itself or simultaneously with the ICE. The MG, by motoring or generating, can also be used to shift the ICE to higher-efficiency operating points. For the P2 architecture, where one MG is placed between the ICE and the gearbox input, a clutch connection also allows the ICE crankshaft to be disengaged from the MG and the rest of the vehicle drivetrain. The parallel P2 HEV layout utilized in this paper is illustrated in Figure 1.

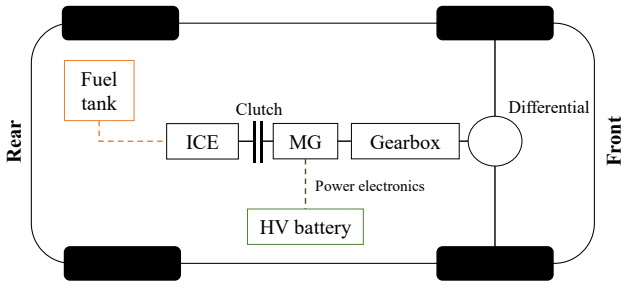

Figure 1. Parallel P2 hybrid powertrain architecture

Series-parallel P1P2

Series-parallel HEV powertrain architectures utilize two MGs. For the P1P2 layout, one MG is located in the P2 position and an additional MG is mounted directly on the ICE crankshaft as shown in Figure 2. When the clutch is engaged, the ICE, MG1 and MG2 exhibits the same angular speed and the propelling torque can be arbitrarily distributed among these three power components. On the other hand, when the clutch is disengaged, the HEV powertrain can either operate in pure electric mode (i.e. ICE and MG1 are not activated) or in series mode (i.e. the ICE is turned on and MG1 serves as a generator, providing electrical energy to the battery and MG2).

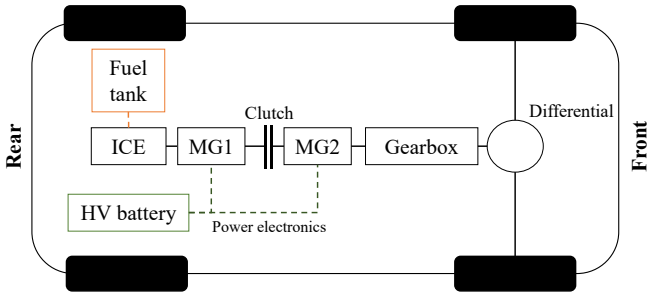

Figure 2. Series-parallel P1P2 hybrid powertrain architecture

Power-split

Power-split HEV architectures have been commercially successful and represent a large portion of the current population of vehicles with full HEV powertrains. They consist of one or multiple planetary gear (PG) sets, which are very compact and function as a continuously variable transmission. PG sets embed a ring gear, a sun gear and a carrier, and they constitute the power-split device, which is responsible for directing the power flow between the components of the hybrid powertrain [22]. Thanks to the PG kinematics, in a power-split HEV the rotating speed of the ICE can be decoupled from the speed of the vehicle, thus enhancing FE potential and flexibility of operation. The power-split HEV layout used in this paper is illustrated in Figure 3 and is the same as that used in the well-known Toyota Hybrid System® [23]. In this HEV configuration, the ICE, MG1 and output shaft to the differential are respectively linked to the carrier, sun gear and ring gear of a PG set, while the MG2 is directly linked to the output shaft through a reduction gearset.

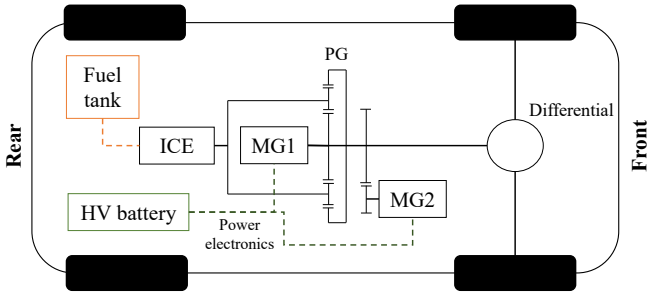

Figure 3. Power-split hybrid powertrain architecture

Vehicle and Powertrain Modeling

In this section, data and parameter values for the modeled vehicle are firstly presented. The adopted HEV powertrain modeling approach is then described. The HEV powertrain architectures are modeled with MATLAB® software.

Vehicle data

Table 1 lists the vehicle and powertrain data used in this paper. The vehicle chassis data, including the mass, tire radius, and road load

coefficients, is for an A-segment passenger car from the US Environmental Protection Agency (EPA) database [24]. The ICE data is for a 3 cylinder in-line naturally aspired spark-ignition engine, and data including an efficiency map is generated by means of the methodology implemented in Amesim® software and described in [25]. Lookup tables for MG efficiency have been derived from [26] and scaled appropriately in order to get a hybridization factor (i.e. the ratio between the total power of the MGs and the overall power available from both ICE and MGs) of around 0.45 for all three of the considered HEV architectures [27]. The battery pack has been modeled as consisting of quantity 200 A123 26650 cells in 100S 2P configuration, thus achieving a nominal capacity of 1.52 kWh. Battery SOC dependent parameters are directly derived from the constant power discharge characteristics for a similar cell in the cell manufacturer's catalogue [28]. Finally, a constant auxiliary loss power of 200 W is assumed which accounts for fluid pumps, lighting, and other auxiliary power requirements.

HEV modeling

In general, a backward quasi-static approach (QSA) is used when modeling the HEV powertrain for solving the off-line optimal control problem which will be detailed later. QSA considers constant time intervals (usually of 1 second) and works back-ward to derive the value of the required propelling torque from vehicle speed values in adjacent time points [29]. This leads to an increase in the computational efficiency in exploring the possible control actions for the HEV powertrain architectures while neglecting transient phenomena in powertrain dynamics. Particularly, the value of required torque at the input shaft of the differential T_{IN} can be determined at each time instant of the driving mission as:

$$T_{IN} = \frac{(F_{roll} + F_{misc} + F_{aero} + m_{veh} \cdot \ddot{x}) \cdot r_{dyn}}{i_{FD}} = \frac{(RL_A + RL_B \cdot \dot{x} + RL_C \cdot \dot{x}^2 + m_{veh} \cdot \ddot{x}) \cdot r_{dyn}}{i_{FD}} \quad (1)$$

where m_{veh}, $\ddot{x}$, r_{dyn} and i_{FD} respectively represent the vehicle mass, the vehicle acceleration (as evaluated from values of vehicle speed in adjacent time instants), the wheel dynamic radius and the final drive ratio. F_{roll}, F_{misc} and F_{aero} are resistive load terms provided by the rolling resistance, some miscellaneous terms (e.g. transmission losses, side forces, road slope) and aerodynamic drag, respectively. As common practice, equation (1) can be consequently rephrased featuring the vehicle speed $\dot{x}$ and three road load coefficients (namely RL_A, RL_B and RL_C) that can be experimentally determined based on vehicle coast down tests.

After T_{IN} is known, the torque acting on each power component is determined by means of torque balance relationships. Following the backward QSA, equations (2), (3) and (4) can be respectively considered for the P2, the P1P2 and the power-split HEV architectures at the generic time instant *j*.

$$T_{ICE} + T_{MG} = \frac{T_{IN}}{i_{gear}(j) \cdot \eta_{TR}^{sign(T_{IN})}} \quad (2)$$

$$T_{ICE} + T_{MG1} + T_{MG2} = \frac{T_{IN}}{i_{gear}(j) \cdot \eta_{TR}^{sign(T_{IN})}} \quad (3)$$

$$\begin{bmatrix} T_{MG1} \\ T_{MG2} \end{bmatrix} = \begin{bmatrix} 0 & -\frac{1}{i_{PG}+1} \\ i_{TG} & -(\frac{i_{PG}}{i_{PG}+1}) \cdot i_{TG} \end{bmatrix} \begin{bmatrix} \frac{T_{IN}}{\eta_{TR}^{sign(T_{IN})}} \\ T_{ICE} \end{bmatrix} \quad (4)$$

T_{ICE}, T_{MG1} and T_{MG2} relate to the values of torque provided by the ICE, the MG1 and the MG2 respectively. It should be noted that the efficiency of the transmission system (η_{TR}) at the denominator of the torque at the input shaft of the differential taken to the power of the sign of T_{IN} in order to account for both motoring and braking operations. η_{TR} is assumed having a constant value here. For the P2 and the P1P2 layout, ICE and MGs torques are additive and i_{gear} is retained as the transmission ratio corresponding to the gear engaged at time instant *j*. For the P1P2 HEV, equation (3) considers the clutch engaged and all the three power components transferring torque to the gearbox. When the clutch is disengaged, only T_{MG2} is considered in the torque balance, while T_{MG1} can be determined by reversing the sign of T_{ICE}, which represents a control variable. On the other hand, for the power-split hybrid powertrain architecture modeled in equation (4), torque values for the MGs can be determined from T_{IN} and T_{ICE} following the constraints for standard epicyclic gearing. In this case, i_{PG} and i_{TG} respectively represent gear ratios for the PG (i.e. ratio between the number of teeth of the ring gear and the number of teeth of the sun gear) and the transfer gearset between MG2 and differential input shaft.

For the electrical energy path, the amount of power that the battery is requested to either deliver or absorb (P_{batt}) is calculated as:

$$P_{batt} = (\sum_{i=1}^{2} \frac{P_{MGi}}{[\eta_{MGi}(\omega_{MGi}, T_{MGi})]^{sign(P_{MGi})}}) + P_{aux} \quad (5)$$

where P_{MG} and η_{MG} respectively represent the mechanical power and the overall efficiency of a MG, which is evaluated by means of empirical lookup tables with speed and torque as independent variables. Taking η_{MG} to the power of the sign of P_{MG} allows capturing both depleting and charging battery conditions within this formula. Both MGs are considered in equation (5) for the P1P2 and the power-split HEV layouts, while a single MG is used for the parallel P2 architecture. Finally, P_{aux} is the auxiliary loss power. The rate of battery SOC change can then be evaluated by considering an equivalent open circuit model as in equation (6):

$$\dot{SOC} = \frac{V_{OC}(SOC) - \sqrt{[V_{OC}(SOC)]^2 - 4 \cdot R_{IN}(SOC) \cdot P_{batt}}}{2 \cdot R_{IN}(SOC)} \cdot \frac{n_p}{Ah_{batt} \cdot 3600} \quad (6)$$

where R_{IN} and V_{OC} are the internal resistance and the open-circuit voltage (OCV) of the battery pack, as obtained by interpolating in 1D lookup tables with SOC as an independent variable. Ah_{batt} is the battery pack capacity in amp-hours, while n_P stands for the number of cells in parallel as given by the battery pack configuration.

Concerning the ICE, the instantaneous rate of fuel consumption can be finally evaluated using an empirical steady-state lookup table with torque and speed as independent variables.

Table 1. Vehicle and hybrid powertrain architectures data.

Component	Parameter	Value
Vehicle	Mass (m_{veh})	1248 kg
	Wheel dynamic radius (r_{dyn})	0.273 m
	Road Load coefficient A (RL_A)	143 N
	Road Load coefficient B (RL_B)	0.90 N/(m/s)
	Road Load coefficient C (RL_C)	0.44 N/(m/s)^2
ICE	Capacity	1.0 l
	Configuration	3 cylinders, in-line
	Type	Spark ignition, naturally aspired

	Maximum power	88 kW @ 5750 rpm
	Maximum torque	190 Nm @ 1750 rpm
Transmission (P2 and P1P2)	Gear ratios (i_{gear})	[3.57 ; 1.92 ; 1.25 ; 0.93 ; 0.75]
	Final drive ratio (i_{FD})	2.92
	Efficiency (η_{TR})	0.9
Transmission (power-split)	PG ratio (ring/sun) (i_{PG})	2.6
	MG2 to output shaft ratio (i_{TG})	1.26
	Final drive ratio (i_{FD})	3.27
	Efficiency (η_{TR})	0.85
MG (P2)	Maximum power	72 kW
	Maximum torque	240 Nm
MG1 (P1P2 and power-split)	Maximum power	22 kW
	Maximum torque	74 Nm
MG2 (P1P2 and power-split)	Maximum power	50 kW
	Maximum torque	167 Nm
Battery pack	Configuration	100S 2P
	Nominal capacity (Q_{batt})	1.52 kWh
	Cell type & capacity	A123 26650, 2.2Ah

Battery ageing model

In this paper, a throughput-based macroscale battery capacity fade model from [16] is employed. This numerical model supposes that a specific amount of charge throughput, which is a function of the current magnitude and temperature of the charge / discharge cycles, can be provided by the battery under steady operating conditions before reaching its end-of-life. Compared to more complex battery ageing models (e.g. electrochemical models and event-based models), throughput-based ageing models exhibit significantly improved computational efficiency [30]. For this reason, they seem to be the most suitable battery ageing models to be implemented in optimization based off-line HEV EMSs as these usually are computationally demanding. The SOH of the high-voltage battery at the generic time instant t_i is defined according to equation (7):

$$SOH(t_i) = SOH_0 - \frac{1}{\int_0^{t_i} \frac{N(c,T)}{c}\,dt} \tag{7}$$

where SOH_0 denotes the initial SOH (equal to 1). c represents the instantaneous battery C-rate, which is defined as the ratio between the current in amps and the battery capacity in amp-hours. N is the number of roundtrip cycles before the battery reaches its end-of-life and it is not a constant value, rather it depends on the battery operating conditions (i.e. C-rate, temperature T). In general, the battery reaches its end-of-life as SOH approaches zero and the battery has no remaining capacity, or when it can no longer perform the function it is intended for. In order to determine N, the percentage of battery capacity loss $\Delta Ah_{batt\%}$ needs to be characterized by following the approach proposed by Bloom et al. in 2001 [31]. This takes inspiration from the Arrhenius equation describing the behavior of ideal gases. However, the general equation has been modified as follows in order to apply it to battery ageing:

$$\Delta Ah_{batt\%} = B(c) \cdot e^{-\frac{A_f(c)}{R \cdot T}} \cdot {Ah_{tp}}^z \tag{8}$$

Following equation (8), $\Delta Ah_{batt\%}$ depends on an empirical pre-exponential factor B, the ageing factor A_f, the lumped cell temperature T, a power-law factor z and the total lifetime throughput Ah_{tp} in ampere-hour. Here, both B and A_f are a function of the instantaneous battery C-rate c. The numerical values for parameters of an A123 26650 cell are obtained from [16], where the authors declared that the numerical model was in turn tuned according to data published in [32]. Table 2 reports parameter values considered here, including the pre-exponential factor B tabulated with respect to c. The lumped cell temperature is assumed to be a constant value of 25°C (i.e. the battery conditioning system maintains this temperature).

Table 2. Battery ageing parameters for a A123 ANR26650 cell.

Parameter	Symbol	Value	Units of measure
Ageing factor	A_f	3814.7 – 44.6·c	K
Power law factor	z	0.55	-
Temperature	T	298	K
Empirical pre-exponential factor, function of current C-rate	B (c=1)	28314	-
	B (c=2)	21681	-
	B (c=6)	12934	-
	B (c=10)	15512	-

The battery ageing model utilized here considers that the end of the HEV BL corresponds to a loss of 20 % of the battery initial capacity, so a value of 20% is used for $\Delta Ah_{batt\%}$. By using this information and solving equation (8) for Ah_{tp}, it becomes possible to calculate the total number of roundtrip cycles allowed for the BL as function of the c-rate in equation (9).

$$N(c,T) = \frac{Ah_{tp}(c,T)}{2 \cdot Ah_{batt}} \tag{9}$$

The factor of two in the denominator allows the model to account for both charging and discharging phases in the battery roundtrip cycles. As an additional hypothesis, the battery ageing model is assumed here to be independent from the battery SOC value. This is likely the case for this application because the HEV powertrains are controlled to operate in charge-sustaining mode, where the battery SOC undertakes a narrow span of values. Predicting the residual BL becomes thus possible using the described model.

Multitarget HEV off-line control problem

This section details the multitarget HEV off-line control problem considering both FE and BL for each of the considered hybrid powertrain architectures. The optimal off-line control problem for an HEV aims here to minimize a multi-objective cost function J that considers estimated fuel consumption, number of ICE activations and BL consumption over a certain period. The resulting mathematical formulation is stated in equation (10):

$$\min\left\{ J = \int_{t_0}^{t_{end}} \mathrm{L}(t)dt \right\}$$

subject to:

$$\begin{gathered} SOC(t_0) = SOC(t_{end}) \\ \dot{SOC} = f(SOC, \omega_{MG1}, T_{MG1}, \omega_{MG2}, T_{MG2}) \\ \omega_{ICE_{min}} \leq \omega_{ICE} \leq \omega_{ICE_{MAX}} \\ \omega_{MG1_{min}} \leq \omega_{MG1} \leq \omega_{MG1_{MAX}} \\ \omega_{MG2_{min}} \leq \omega_{MG2} \leq \omega_{MG2_{MAX}} \end{gathered} \tag{10}$$

$$T_{ICE_{min}} \leq T_{ICE} \leq T_{ICE_{MAX}}$$
$$T_{MG1_{min}} \leq T_{MG1} \leq T_{MG1_{MAX}}$$
$$T_{MG2_{min}} \leq T_{MG2} \leq T_{MG2_{MAX}}$$
$$SoC_{min} \leq SoC \leq SoC_{MAX}$$
$$SoH_0 = 1$$

Where $L(t)$ represents the instantaneous cost function. The sustenance of the battery SOC is defined by imposing equivalent battery SOC values at the beginning and the end of the considered time period. Both battery SOC, speeds ω and torques T of power components are restricted within the corresponding actual operating regions. The initial battery SOH is set to 1 in order to consider non-aged battery conditions. The instantaneous cost function $L(t)$ can then be stated in equation (11).

$$L(t) = \left[\dot{m}_{fuel} + m_{fuel_{start}} \cdot (start_{ICE} > 0)\right] \cdot \$_{fuel} + \alpha_{batt} \cdot \$_{batt} \cdot \dot{SoH}] \quad (11)$$

$\dot{m}_{fuel}$ and $m_{fuel_{start}}$ represent the fuel mass rate at each time instant in which the ICE operates and the amount of fuel mass needed to crank the ICE throughout starting events, respectively. $start_{ICE}$ defines a binary variable detecting ICE start occurrence. The variables $\$_{fuel}$ and $\$_{batt}$ represent cost values for fuel and for the battery, respectively. The variable $\$_{fuel}$ is based on the January 2020 averaged US gasoline price of 2.62 \$/gallon [33], while a value of \$3000 is used for $\$_{batt}$ from [34]. $\dot{SoH}$ is the instantaneous rate of battery SOH, while α_{batt} denotes a reliability coefficient for the illustrated battery ageing model. The higher the α_{batt} value, the less trust is given to the illustrated ageing model and the more the battery ageing effect is constrained at the expense of FE.

In the follow-up of this section, DP will be illustrated as a numerical approach to solve the illustrated control problem.

Dynamic programming

DP is by far the most adopted approach for solving HEV optimal control problems. It involves generating a globally optimal solution backward along a time horizon by searching through all feasible discrete control actions for all the state grid points [35][36]. While DP is demonstrated achieving global optimality under a wide range of operating conditions, its major drawback is the computational power and time needed to solve the grid of solutions and search for the optimal path through the solution space [6]. The DP state variable set X considered here is reported in equation (12).

$$X = \begin{Bmatrix} SOC \\ ICE_{on/off} \end{Bmatrix} \quad (12)$$

The battery SOC is used as a state variable in order to achieve charge-sustained operation, while a binary term defining the ICE state (i.e. on/off) is considered in order to account for comfort and smooth HEV operation. ICE cranking events are detected thanks to changes in the state term for the ICE state. A third state variable term could theoretically be considered here for the battery SOH. However, since DP dimensionality increases exponentially with additional state variable terms, this would result in a dramatic increase of both computational time, computational power and storage memory required. To avoid this drawback, as it will be described later, a sweep of the coefficient α_{batt} is performed instead. The control variables will be detailed below for each of the investigated HEV powertrain architectures.

Parallel P2

When controlling a parallel P2 HEV, three levels of decisions need to be made at each time instant:

1. Which gear is to be engaged in the gearbox;
2. Whether to propel the HEV in pure electric mode (MG only) or in hybrid operation (both ICE and MG operating);
3. In case the hybrid mode is selected, how is the required torque split between the ICE and MG.

This leads to the use of two terms, as illustrated in equation (13), for the control variable U_{P2}, including the gear number n_{gear} and the value of ICE torque T_{ICE}.

$$U_{P2} = \begin{Bmatrix} n_{gear} \\ T_{ICE} \end{Bmatrix} \quad (13)$$

In a backward HEV modelling approach, pure electric or hybrid operation are distinguished by ICE torque being zero or positive, respectively.

Series-parallel P1P2

The required control decisions for a series-parallel P1P2 layout are similar to the ones for the parallel P2 HEV architecture, yet a few additions need to be made. The decisions necessary are as follows:

1. Which gear is to be engaged in the gearbox;
2. Whether to keep the clutch engaged or disengaged;
3. In case the clutch is engaged, how to split the required torque between ICE, MG1 and MG2;
4. In case the clutch is disengaged, whether to operate in pure electric mode (i.e. only MG2 is activated) or in series mode (ICE and MG1 are activated as well);
5. When series hybrid operation is selected, which values of speed and torque to assign to the ICE and MG1.

As a result, the corresponding control variable U_{P1P2} requires additional terms to handle the increased control complexity for this HEV layout, namely the MG1 torque T_{MG1}, the ICE speed ω_{ICE} and the binary clutch status $Cl_{eng/dis}$ (i.e. engaged or disengaged) as in equation (14).

$$U_{P1P2} = \begin{Bmatrix} \mathrm{n}_{gear} \\ T_{ICE} \\ T_{MG1} \\ \omega_{ICE} \\ Cl_{eng/dis} \end{Bmatrix} \quad (14)$$

Power-split

Power-split HEV powertrain architectures exhibit different terms in their control variables compared to parallel and series-parallel layouts. The control variable U_{PS} considered in this paper for the power-split HEV layout thus contains speed and torque values for the ICE as formulated in equation (15).

$$U_{PS} = \begin{Bmatrix} \omega_{ICE} \\ T_{ICE} \end{Bmatrix} \quad (15)$$

In a backward modeling approach, values of speed and torques for both the MGs can indeed be evaluated starting from the control variable terms following the planetary gear kinematics and dynamics [22]. In the considered power-split HEV layout, a gearbox is not strictly necessary in the hybrid transmission because the PG sets operate as an electrically variable transmission (eVT).

Results

In this section, results are discussed for the simulated HEV powertrain architectures which are controlled off-line following the multitarget DP approach introduced in the last section. Seven driving missions are simulated here including standard drive cycles consisting of the urban dynamometer driving schedule (UDDS), the highway federal test procedure (HWFET), the new European driving cycle (NEDC), the worldwide harmonized light vehicle test procedure (WLTP) and the US06 Supplemental Federal Test Procedure (US06), and real-world driving missions recorded by the authors in Langhe, a hilly area in Piedmont, northern Italy, including extra-urban uphill (RWC_uphill) and extra-urban downhill driving conditions (RWC_downhill) respectively ~~[36]~~. Recorded vehicle speed and GPS altitude profiles for these two real-world driving missions are illustrated in Figure 4.

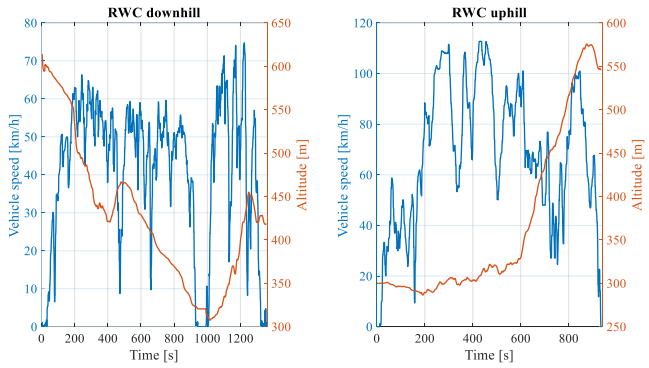

Figure 4. Retained real-world driving missions.

All the listed driving missions have been simulated for all the three of the considered hybrid powertrain architectures while being controlled off-line by the multi-objective DP approach. The grid for each control variable term related to speed or torque of components has been created with 30 elements, while the grid for the state variable term related to SOC has been created with 1000 elements. Following the detailed DP control approach, the required computational times to simulate a driving mission on a desktop computer with an Intel Core i7-8700 (3.2 GHz) processor and 32 GB of RAM amounts to approximately 30, 60 and 120 minutes for the parallel P2, the power-split and the series-parallel P1P2 HEV architectures, respectively. Initially, a simulation considering only FE maximization is performed by setting the value of α_{batt} to 0. An example of time domain results obtained for a selected portion of the WLTP cycle is shown in Figure 5 for each of the analyzed hybrid powertrain layouts including ICE power, MGs power, battery power and total transmission mechanical power. Then, the coefficient α_{batt} is tuned to gradually increase the estimated BL up to around 300 thousand km. The battery lifetime in kilometers is evaluated here by considering the corresponding driving mission as steadily repeated over the entire vehicle lifetime. In this case, an example of time domain battery power and SOC results obtained for US06 considering different optimization goals (OGs) is displayed in Figure

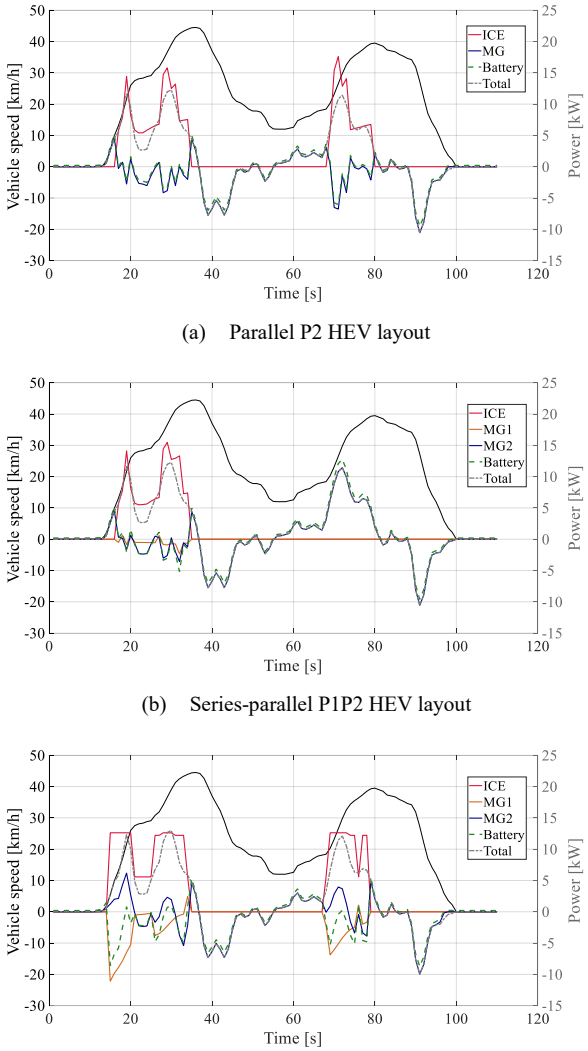

(a) Parallel P2 HEV layout

(b) Series-parallel P1P2 HEV layout

(c) Power-split HEV layout

Figure 5. Optimal HEV operation predicted by DP for selected portion of WLTP.

6 including FE only, BL of 200 thousand km and BL of 300 thousand km for all the HEV configurations under analysis.

The fuel economy of each HEV architecture for the FE

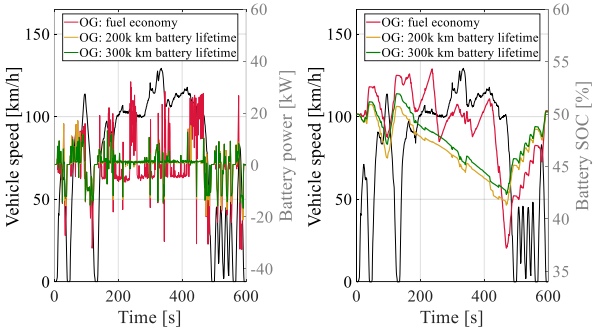

(a) Parallel P2 HEV layout

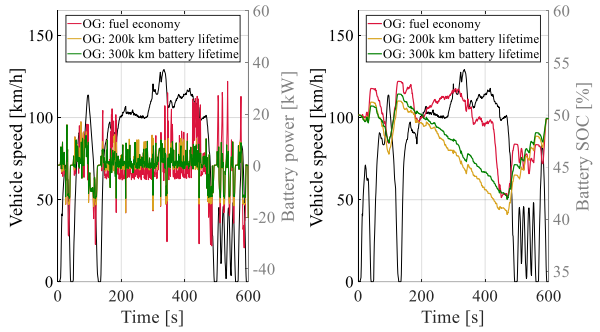

(b) Series-parallel P1P2 HEV layout

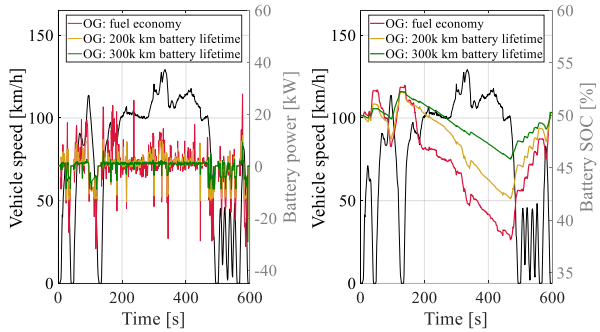

(c) Power-split HEV layout

Figure 6. Battery power and SOC as predicted by the multi-objective DP in US06 for different optimization goals.

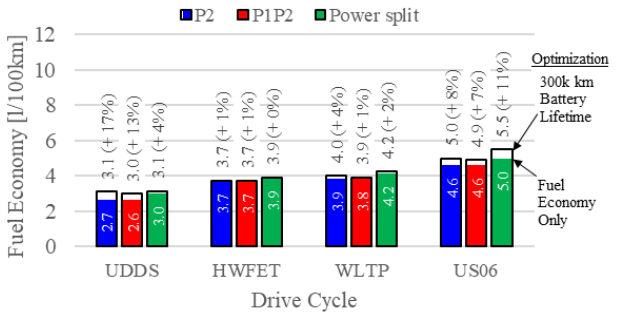

Figure 7. Fuel economy for selected driving missions considering FE only and 300 thousand km BL optimization goals.

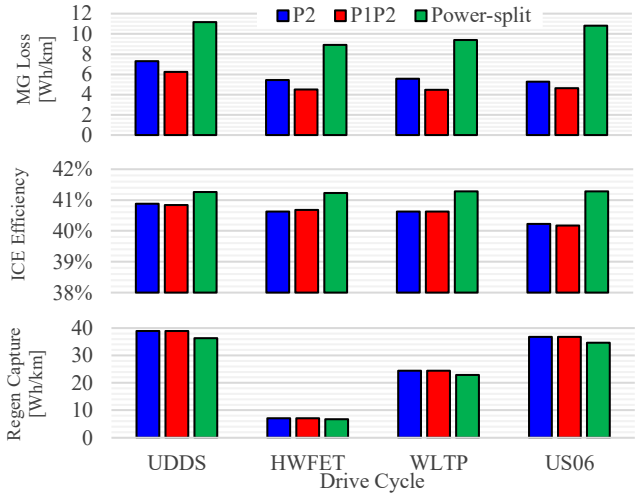

Figure 8. Motor generator loss, ICE efficiency, and regenerative braking energy captured for fuel economy only case and selected driving missions.

and 300k km BL cases is shown in Figure 7 for selected drive cycles. This shows that the P1P2 system has the best fuel economy, followed by the P2 and power-split case. While the power-split case does allow for the engine speed to be decoupled from the wheels thus enhancing its efficiency, this results in higher motor generator loss due to power circulating through the system, as is illustrated in Figure 8 along with ICE efficiency and captured regenerative braking energy for each case. When the system control is optimized for a BL of 300k km, fuel economy does not change for the HWFET case, increases a few percent for the more aggressive WLTP and US06 cases, and increases as much as 17% for the UDDS city driving case where many starts and stops are performed. When controlling for 300k km BL, each HEV architecture loses more than 4.9% fuel economy for at least one drive cycle, making it unclear if any of the investigated architectures have advantages regarding battery lifetime.

Pareto frontiers for obtained simulation results considering FE and BL are illustrated in Figure 9, where the three HEV powertrain architectures are compared in each considered driving mission. In Appendix 1, Table 3, Table 4 and Table 5 report numerical results for breakpoints corresponding to OGs of FE solely, estimated BL of 200 thousand km and estimated BL of 300 thousand km for parallel P2, series-parallel P1P2 and power-split hybrid powertrain architectures, respectively. For 200k km BL and 300k km BL cases, variations in FE (Δ FE) and BL (Δ BL) are reported and compared with the FE only optimization case. Particularly, differences in FE are reported in percentage points, while variations in BL are expressed in multiples of FE battery lifetime.

Overall, obtained results suggest that achieving a satisfactory BL is generally not possible when optimizing for fuel economy only for the modeled hybrid powertrain component size values. When setting the value of α_{batt} to 0, BL ranges from 14 thousand km to 128 thousand km for the parallel P2, from 11.3 thousand km to 164.3 thousand km for the series-parallel P1P2 and from 15 thousand km to 182 thousand km for the power-split HEV powertrain architectures, respectively. A remarkable increase in the BL can be achieved with a small reduction of FE depending on the driving mission and the hybrid powertrain configuration. For example Table 3 in the appendix shows that for the P2 HEV, the multitarget DP control extends BL 3.0 times for HWFET and 2.7 times for NEDC with only a 1.2% and 0.6 % reduction in fuel economy. For the series-parallel P1P2 layout performing the WLTP and HWFET cycles, the BL is

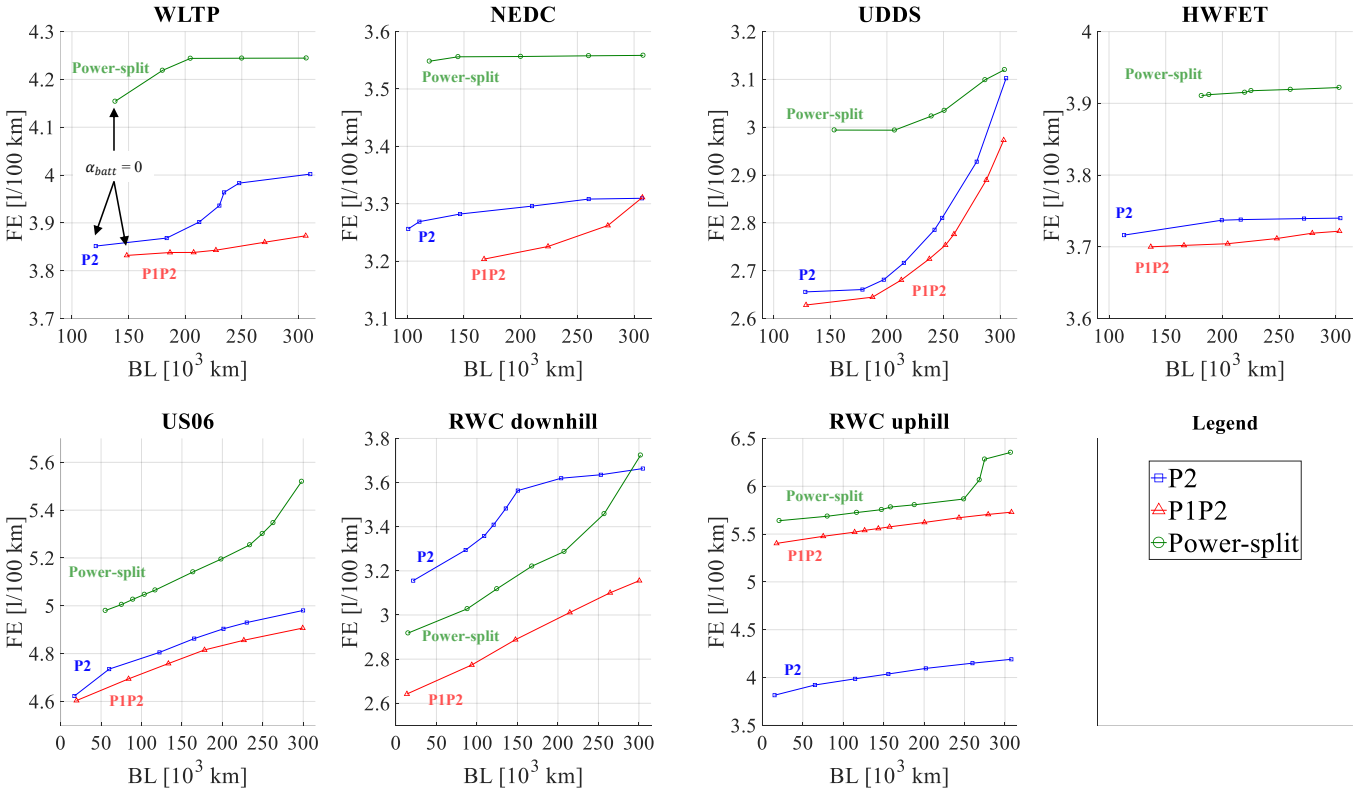

Figure 9. Pareto frontiers for FE and BL as obtained by the multi-objective DP over considered driving missions.

doubled while worsening the corresponding FE respectively by only 1% and 0.5% for the 300 thousand km BL target. Finally, the developed multi-target control approach for the power-split HEV, as shown in Table 5 in the appendix, appears remarkably effective in NEDC and HWFET as for the P2 HEV since the BL can be extended respectively 2.6 times and 1.7 times while worsening the corresponding FE by only 0.3 % for the 300 thousand km BL target.

To give further insight into each hybrid powertrain's performance, several additional operational statistics for the modeled cases are listed in Table 6, Table 7 and Table 8 in the appendix. In general, a gradual decrease in the percentage of time spent in pure electric operation can be observed for all the HEV layouts and driving missions when the controller is tuned to increase BL. Moreover, consistent reductions are achieved both in terms of SOC window utilization (i.e. the difference between the highest and the lowest values of SOC observed throughout the retained driving missions) and root mean square (RMS) battery cell current. Furthermore, a remarkable increase can be observed for braking energy dissipated by the friction brakes, correlating with a decrease in the kinetic energy converted into electrical energy and stored in the battery during braking. This suggests a need for dedicated regenerative braking control strategies capable of coordinating electrical braking and friction braking in order to find the best trade-off between electrical energy recovery and BL preservation. From a component loss perspective, observed electrical loss for the MGs usually decreases when gradually increasing the estimated BL. This correlates well with the reduction in the SOC window, which in turn implies a decrease in the cumulative battery charge/discharge power.

Conclusions

This work investigates the optimal performance of different HEV powertrain architectures when considering both FE and BL as optimization targets. A multiobjective DP formulation is developed as an off-line optimal HEV control approach. Then, its application is extended to parallel P2, series-parallel P1P2 and power-split hybrid powertrain layouts.

Obtained results suggest that the developed multitarget optimal control approach can effectively extend the predicted BL by several times over a wide range of driving conditions while limiting the overall increase in predicted fuel consumption. From an OEM perspective, a dedicated hybrid powertrain control approach could be preferred in this way rather than upsizing the HV battery to achieve the desired BL target. Significant benefits could be achieved in this way both in terms of overall HEV cost and performance.

Among the investigated HEV powertrain architectures, the P1P2 exhibits the highest performance in terms of FE for almost all of the cases investigated. Nevertheless, it should be noted that this statement might change if component sizing was considered as well in the analysis. In general, when considering BL targets as well, control actions performed by DP tend to reduce the depth of discharge of the battery over the driving missions. Moreover, the percentage of time spent in pure electric operation is reduced in favor of hybrid electric operation (either power assist or battery charging based). Furthermore, the amount of braking energy dissipated by means of friction brakes is increased when extending BL. Finally,

ranking of HEV powertrain layout options has been made possible by considering both FE and BL as parameters for the analysis.

Future work could consider the implementation of the proposed multitarget DP approach in sizing procedures for HEV powertrain architectures. Moreover, on-line battery sensitive supervisory controllers for HEV powertrains could be developed and calibrated based on the proposed optimal off-line control approach. Finally, attention should be paid to integrate BL consideration in the development of dedicated control strategies for regenerative braking in electrified vehicles.

References

1. B. Bilgin et al., "Making the Case for Electrified Transportation," in *IEEE Transactions on Transportation Electrification*, vol. 1, no. 1, pp. 4-17, 2015.
2. P.G. Anselma, G. Belingardi, "Comparing battery electric vehicle powertrains through rapid component sizing", *Int. J. Electric and Hybrid Vehicles*, vol.11, no.1, pp. 36-58, 2019.
3. A. Biswas, A. Emadi, "Energy Management Systems for Electrified Powertrains: State-of-the-Art Review and Future Trends," in *IEEE Transactions on Vehicular Technology*, vol. 68, no. 7, pp. 6453-6467, July 2019.
4. Millo, F., Badami, M., Ferraro, C., and Rolando, L., "Different Hybrid Powertrain Solutions for European Diesel Passenger Cars," *SAE Int. J. Engines* 2(2):493-504, 2010.
5. G. Belingardi, P.G. Anselma, M. Demic, "Optimization-based controllers for hybrid electric vehicles", in *Mobility & Vehicle Mechanics*, vol. 44, no. 3, pp. 53-67, 2018.
6. J. Lempert, B. Vadala, K. Arshad-Aliy, J. Roeleveld and A. Emadi, "Practical Considerations for the Implementation of Dynamic Programming for HEV Powertrains," *2018 IEEE Transportation Electrification Conference and Expo (ITEC)*, Long Beach, CA, 2018, pp. 755-760.
7. N. Kim, S. Cha and H. Peng, "Optimal Control of Hybrid Electric Vehicles Based on Pontryagin's Minimum Principle," in *IEEE Transactions on Control Systems Technology*, vol. 19, no. 5, pp. 1279-1287, 2011.
8. P.G. Anselma, Y. Huo, E. Amin, J. Roeleveld, A. Emadi, G. Belingardi, "Mode-shifting Minimization in a Power Management Strategy for Rapid Component Sizing of Multimode Power-split Hybrid Vehicles," *SAE Technical Paper* 2018-01-1018, 2018.
9. P. G. Anselma, Y. Huo, J. Roeleveld, G. Belingardi and A. Emadi, "Slope-Weighted Energy-Based Rapid Control Analysis for Hybrid Electric Vehicles," in *IEEE Transactions on Vehicular Technology*, vol. 68, no. 5, pp. 4458-4466, 2019.
10. S. Amirfarhangi Bonab and A. Emadi, "Fuel-Optimal Energy Management Strategy for a Power-Split Powertrain via Convex Optimization," in *IEEE Access*, vol. 8, pp. 30854-30862, 2020.
11. Finesso, R., Spessa, E., and Venditti, M., "Cost-Optimized Design of a Dual-Mode Diesel Parallel Hybrid Electric Vehicle for Several Driving Missions and Market Scenarios," *Applied Energy*, 177:366, 2016.
12. P.G. Anselma, G. Belingardi, A. Falai, C. Maino, F. Miretti, D. Misul, E. Spessa, "Comparing Parallel Hybrid Electric Vehicle Powertrains for Real-world Driving", *2019 AEIT International Conference of Electrical and Electronic Technologies for Automotive*, Torino, Italy, 2019, pp. 1-6.
13. Anselma, P.G. and Belingardi, G., "Next Generation HEV Powertrain Design Tools: Roadmap and Challenges," SAE Technical Paper 2019-01-2602, 2019.
14. P. J. Kollmeyer, T. M. Jahns, "Aging and performance comparison of absorbed glass matte, enhanced flooded, PbC, NiZn, and LiFePO4 12V start stop vehicle batteries", *J. Power Sources*, vol. 441, 2019.
15. A. Bonfitto, E. Ezemobi, N. Amati, S. Feraco, A. Tonoli and S. Hegde, "State of Health Estimation of Lithium Batteries for Automotive Applications with Artificial Neural Networks," *2019 AEIT International Conference of Electrical and Electronic Technologies for Automotive (AEIT AUTOMOTIVE)*, Torino, Italy, 2019, pp. 1-5.
16. S. Ebbesen, P. Elbert and L. Guzzella, "Battery State-of-Health Perceptive Energy Management for Hybrid Electric Vehicles," in *IEEE Transactions on Vehicular Technology*, vol. 61, no. 7, pp. 2893-2900, Sept. 2012.
17. L. Tang, G. Rizzoni and S. Onori, "Energy Management Strategy for HEVs Including Battery Life Optimization," in *IEEE Transactions on Transportation Electrification*, vol. 1, no. 3, pp. 211-222, Oct. 2015.
18. C. Patil, P. Naghshtabrizi, R. Verma, Zhijun Tang, K. Smith and Ying Shi, "Optimal battery utilization over lifetime for parallel hybrid electric vehicle to maximize fuel economy," 2016 American Control Conference (ACC), Boston, MA, 2016, pp. 1524-1529.
19. Li, J., Huber, T., and Beidl, C., "Predictive Multi-Objective Operation Strategy Considering Battery Cycle Aging for Hybrid Electric Vehicles," *SAE Int. J. Alt. Power.* 7(3):217-232, 2018.
20. S. Xie, X. Hu, Q. Zhang, X. Lin, B. Mu, H. Ji, "Aging-aware co-optimization of battery size, depth of discharge, and energy management for plug-in hybrid electric vehicles", Journal of Power Sources, Vol. 450, 2020.
21. Yang, Y., Ali, K. A., Roeleveld, J., Emadi, A., "State-of-the-art electrified powertrains - hybrid, plug-in, and electric vehicles", in *International Journal of Powertrains*, vol. 5, no.1, pp.1-29, 2016.
22. Schulz M., "Circulating mechanical power in a power split hybrid electric vehicle transmission", Proc IMeche, Part D: J Automobile Engineering, 2004; 218: 1419–1425.
23. Matsumura, M., Shiozaki, K., and Mori, N., "Development of New Hybrid Transaxle for Mid - Size Vehicle," *SAE Technical Paper* 2018-01-0429, 2018.
24. United States Environmental Protection Agency, "Compliance and Fuel Economy Data - Annual Certification Data for Vehicles, Engines, and Equipment", [online] https://www.epa.gov/compliance-and-fuel-economy-data/annual-certification-data-vehicles-engines-and-equipment (accessed 6 April 2020).
25. Alix, G., Dabadie, J., and Font, G., "An ICE Map Generation Tool Applied to the Evaluation of the Impact of Downsizing on Hybrid Vehicle Consumption," *SAE Technical Paper* 2015-24-2385, 2015.
26. Dabadie, J., Sciarretta, A., Font, G., and Le Berr, F., "Automatic Generation of Online Optimal Energy Management Strategies for Hybrid Powertrain Simulation," *SAE Technical Paper* 2017-24-0173, 2017.
27. J. M. Tyrus, R. M. Long, M. Kramskaya, Y. Fertman and A. Emadi, "Hybrid electric sport utility vehicles", *IEEE Transactions on Vehicular Technology* 2004; 53(5): 1607-22.
28. A123 systems, "Nanophosphate® High Power LithiumIon Cell ANR26650M1-B", [online] https://www.batteryspace.com/prod-specs/6610.pdf (accessed 22 January 2020).
29. L. Guzzella and A. Amstutz, "CAE tools for quasi-static modeling and optimization of hybrid powertrains," in *IEEE Transactions on Vehicular Technology*, vol. 48, no. 6, pp. 1762-1769, 1999.

30. Vora, A. P., Jin, X., Hoshing, V., Shaver, G., Varigonda, S., & Tyner, W. E., "Integrating battery degradation in a cost of ownership framework for hybrid electric vehicle design optimization", *Proc IMeche, Part D: J Automobile Engineering*, online 21 Oct. 2018.
31. I. Bloom, B. W. Cole, J. J. Sohn, S. A. Jones, E. G. Polzin, V. S. Battaglia, G. L. Henriksen, C. Motloch, R. Richardson, T. Unkelhaeuser, D. Ingersoll, and H. L. Case, "An accelerated calendar and cycle life study of Li-ion cells," *J. Power Sources*, vol. 101, no. 2, pp. 238–247, Oct. 2001.
32. J. Wang, P. Liu, J. Hicks-Garner, E. Sherman, S. Soukiazian, M. Verbrugge, H. Tataria, J. Musser, and P. Finamore, "Cycle-life model for graphite- LiFePO4 cells," *J. Power Sources*, vol. 196, no. 8, pp. 3942– 3948, Apr. 2011.
33. US Department of Energy, "eGallon: Compare the costs of driving with electricity", [online] https://www.energy.gov/maps/egallon (accessed 19 January 2020).
34. L. Serrao, S. Onori, A. Sciarretta, Y. Guezennec and G. Rizzoni, "Optimal energy management of hybrid electric vehicles including battery aging," *Proceedings of the 2011 American Control Conference*, San Francisco, CA, 2011, pp. 2125-2130.
35. O. Sundstrom and L. Guzzella, "A generic dynamic programming Matlab function," *2009 IEEE Control Applications, (CCA) & Intelligent Control, (ISIC)*, St. Petersburg, 2009, pp. 1625-1630.
36. Bruck, L., Lempert, A., Amirfarhangi Bonab, S., Lempert, J. et al., "A Dynamic Programming Algorithm for HEV Powertrains Using Battery Power as a State Variable," SAE Technical Paper 2020-01-0271, 2020.

Contact Information

Pier Giuseppe Anselma

Department of Mechanical and Aerospace Engineering (DIMEAS), Center for Automotive Research and Sustainable Mobility (CARS), Politecnico di Torino, Corso Duca degli Abruzzi 24, 10129 Torino, Italy.

Mail: pier.anselma@polito.it

Definitions/Abbreviations

BEV	Battery electric vehicle
BL	Battery lifetime
BSFC	Brake specific fuel consumption
DP	Dynamic programming
ECMS	Equivalent fuel consumption minimization strategy
EMS	Energy management strategy
eVT	Electrically variable transmission
FE	Fuel economy
HEV	Hybrid electric vehicle
HWFET	Highway fuel economy test
ICE	Internal combustion engine
MG	Motor/generator
OCV	Open circuit voltage
OG	Optimization goal
PEARS	Power-weighted efficiency analysis for rapid sizing
PG	Planetary gear
PMP	Pontryagin's minimum principle
QSA	Quasi-static approach
SERCA	Slope-weighted energy-based rapid control analysis
SOC	State-of-charge
SOH	State-of-health
UDDS	Urban dynamometer driving schedule
WLTP	Worldwide-harmonized Light-vehicle Test Procedure

Appendix 1

Table 3. Numerical results for fuel economy and battery lifetime – P2 HEV.

	OG : fuel economy only (α_{batt} = 0)		OG : battery lifetime of around 200k km (α_{batt} = 0.03 to 0.5)				OG : battery lifetime of around 300k km (α_{batt} = 0.25 to 1.25)			
Driving mission	FE [l/100 km]	BL [10^3 km]	FE [l/100 km]	BL [10^3 km]	Δ FE (FE only) [%]	Δ BL (FE only) [x]	FE [l/100 km]	BL [10^3 km]	Δ FE (FE only) [%]	Δ BL (FE only) [x]
WLTP	3.9	121	3.9	212	+ 1.3%	x 1.8	4.0	310	+ 3.9%	x 2.6
NEDC	3.3	101	3.3	210	+ 1.1%	x 2.1	3.3	307	+ 1.2%	x 3.0

UDDS	2.7	128	2.7	213	+ 0.9%	x 1.7	3.0	303	+ 11.9%	x 2.4
HWFET	3.7	113	3.7	200	+ 0.6%	x 1.8	3.7	304	+ 0.6%	x 2.7
US06	4.6	17	4.9	201	+ 6.1%	x 11.8	5.0	300	+ 7.8%	x 17.6
RWC_downhill	3.2	21	3.6	204	+ 14.7%	x 9.6	3.7	305	+ 16.1%	x 14.3
RWC_uphill	3.8	15	4.1	202	+ 7.3%	x 13.4	4.2	308	+ 9.9%	x 20.4

Table 4. Numerical results for fuel economy and battery lifetime – P1P2 HEV.

	OG : fuel economy only (α_{batt} = 0)		OG : battery lifetime of around 200k km (α_{batt} = 0.01 to 0.2)				OG : battery lifetime of around 300k km (α_{batt} = 0.05 to 0.5)			
Driving mission	FE [l/100 km]	BL [10^3 km]	FE [l/100 km]	BL [10^3 km]	Δ FE (FE only) [%]	Δ BL (FE only) [x]	FE [l/100 km]	BL [10^3 km]	Δ FE (FE only) [%]	Δ BL (FE only) [x]
WLTP	3.8	148	3.8	207	+ 0.2%	x 1.4	3.9	306	+ 1.0%	x 2.1
NEDC	3.2	168	3.2	224	+ 0.9%	x 1.3	3.3	307	+ 3.4%	x 1.8
UDDS	2.6	129	2.7	213	+ 2.0%	x 1.7	3.0	303	+ 13.1%	x 2.3
HWFET	3.7	137	3.7	205	+ 0.0%	x 1.5	3.7	303	+ 0.5%	x 2.2
US06	4.6	20	4.8	178	+ 4.7%	x 9.1	4.9	299	+ 6.7%	x 15.2
RWC_downhill	2.6	14	3.0	215	+ 13.9%	x 15.8	3.2	301	+ 19.4%	x 22.1
RWC_uphill	5.4	18	5.6	200	+ 4.1%	x 11.4	5.7	308	+ 6.1%	x 17.5

Table 5. Numerical results for fuel economy and battery lifetime – Power-split HEV.

	OG : fuel economy only (α_{batt} = 0)		OG : battery lifetime of around 200k km (α_{batt} = 0.02 to 0.2)				OG : battery lifetime of around 300k km (α_{batt} = 0.2 to 2)			
Driving mission	FE [l/100 km]	BL [10^3 km]	FE [l/100 km]	BL [10^3 km]	Δ FE (FE only) [%]	Δ BL (FE only) [x]	FE [l/100 km]	BL [10^3 km]	Δ FE (FE only) [%]	Δ BL (FE only) [x]
WLTP	4.2	138	4.2	205	+ 2.2%	x 1.5	4.2	307	+ 2.2%	x 2.2
NEDC	3.6	119	3.6	200	+ 0.3%	x 1.7	3.6	308	+ 0.3%	x 2.6
UDDS	3.0	154	3.0	207	+ 0.1%	x 1.3	3.1	304	+ 4.3%	x 2.0
HWFET	3.9	182	3.9	188	+ 0.0%	x 1.0	3.9	303	+ 0.3%	x 1.7
US06	5.0	55	5.2	198	+ 4.3%	x 3.6	5.5	298	+ 10.8%	x 5.4
RWC_downhill	2.9	15	3.3	208	+ 12.6%	x 13.9	3.7	302	+ 27.5%	x 20.2
RWC_uphill	5.6	21	5.8	188	+ 2.9%	x 9.0	6.4	307	+ 12.7%	x 14.7

Appendix 2

Table 6. Operational statistics for simulated driving missions – P2 HEV.

Driving mission			Fuel economy only	Battery lifetime of 200 thousand km	Battery lifetime of 300 thousand km
WLTP	Operating mode selection	Pure electric [%]	65.2	55.7	44.9
		Hybrid power assist [%]	7.2	10.4	52.1
		Hybrid battery charging [%]	27.6	33.9	3.0
	SOC window [%]		22.5	8.7	8.4
	Cell current RMS [A]		8.8	5.9	4.4
	Friction brake energy [kJ]		8	59	182
	Regenerative energy [kJ]		2042	1991	1868
	MG electrical loss [kJ]		466	391	349
	ICE averaged BSFC [g/kWh]		206.1	211.7	216.6
NEDC	Operating mode selection	Pure electric [%]	73.2	63.0	60.8
		Hybrid power assist [%]	1.8	6.2	6.2
		Hybrid battery charging [%]	25.0	30.8	33.0
	SOC window [%]		15.9	10.5	9.2
	Cell current RMS [A]		6.9	4.7	4.3
	Friction brake energy [kJ]		8	25	48
	Regenerative energy [kJ]		976	959	936
	MG electrical loss [kJ]		256	199	193
	ICE averaged BSFC [g/kWh]		206.3	213.1	214.1
UDDS	Operating mode selection	Pure electric [%]	76.0	65.1	39.4
		Hybrid power assist [%]	5.2	11.3	55.5
		Hybrid battery charging [%]	18.8	23.6	5.1
	SOC window [%]		14.3	6.8	3.8
	Cell current RMS [A]		8.0	5.9	3.7
	Friction brake energy [kJ]		12	26	381
	Regenerative energy [kJ]		1680	1665	1311
	MG electrical loss [kJ]		316	271	284
	ICE averaged BSFC [g/kWh]		204.8	211.7	227.2
HWFET	Operating mode selection	Pure electric [%]	51.0	36.9	36.3
		Hybrid power assist [%]	1.3	1.7	1.7
		Hybrid battery charging [%]	47.7	61.4	62.0
	SOC window [%]		19.8	11.3	11.2
	Cell current RMS [A]		13.0	8.3	7.9
	Friction brake energy [kJ]		1	8	17
	Regenerative energy [kJ]		421	413	404
	MG electrical loss [kJ]		323	228	224
	ICE averaged BSFC [g/kWh]		206.1	213.2	213.4
US06	Operating mode selection	Pure electric [%]	49.2	28.9	24.1
		Hybrid power assist [%]	14.1	64.7	67.6
		Hybrid battery charging [%]	36.7	6.4	8.4
	SOC window [%]		17.1	9.6	9.6
	Cell current RMS [A]		16.6	9.1	8.1
	Friction brake energy [kJ]		16	393	494
	Regenerative energy [kJ]		1707	1330	1229
	MG electrical loss [kJ]		245	220	212
	ICE averaged BSFC [g/kWh]		208.1	216.5	217.8
RWC_uphill	Operating mode selection	Pure electric [%]	55.7	40.3	34.9
		Hybrid power assist [%]	11.6	21.5	45.9
		Hybrid battery charging [%]	32.6	38.2	19.2

	SOC window [%]		13.3	3.7	4.5
	Cell current RMS [A]		14.8	9.1	7.7
	Friction brake energy [kJ]		153	709	872
	Regenerative energy [kJ]		2405	1848	1685
	MG electrical loss [kJ]		358	295	277
	ICE averaged BSFC [g/kWh]		208.2	216.1	218.5
RWC_downhill	Operating mode selection	Pure electric [%]	67.5	33.2	31.4
		Hybrid power assist [%]	8.4	56.5	58.0
		Hybrid battery charging [%]	24.1	10.3	10.5
	SOC window [%]		10.5	5.4	4.9
	Cell current RMS [A]		12.1	6.0	5.7
	Friction brake energy [kJ]		166	931	938
	Regenerative energy [kJ]		2451	1687	1679
	MG electrical loss [kJ]		366	272	268
	ICE averaged BSFC [g/kWh]		205.9	222.9	223.7

Table 7. Operational statistics for simulated driving missions – P1P2 HEV.

Driving mission			Fuel economy only	Battery lifetime of 200 thousand km	Battery lifetime of 300 thousand km
WLTP	Operating mode selection	Pure electric [%]	65.8	62.5	57.1
		Series [%]	0.2	1.5	1.8
		Hybrid power assist [%]	6.8	9.3	11.6
		Hybrid battery charging [%]	27.3	26.7	29.4
	SOC window [%]		23.6	16.4	8.8
	Cell current RMS [A]		8.9	7.5	6.0
	Friction brake energy [kJ]		8	8	77
	Regenerative energy [kJ]		2042	2042	1973
	MG1 electrical loss [kJ]		2	14	21
	MG2 electrical loss [kJ]		373	337	306
	ICE averaged BSFC [g/kWh]		206.1	208.1	210.3
NEDC	Operating mode selection	Pure electric [%]	74.7	66.8	59.0
		Series [%]	0.0	0.0	0.0
		Hybrid power assist [%]	1.8	4.8	7.7
		Hybrid battery charging [%]	23.6	28.4	33.3
	SOC window [%]		18.1	13.7	7.1
	Cell current RMS [A]		7.1	5.3	4.1
	Friction brake energy [kJ]		10	24	83
	Regenerative energy [kJ]		974	960	901
	MG1 electrical loss [kJ]		1	7	14
	MG2 electrical loss [kJ]		208	172	154
	ICE averaged BSFC [g/kWh]		205.8	210.4	214.9
UDDS	Operating mode selection	Pure electric [%]	76.6	65.2	47.1
		Series [%]	0.2	2.4	4.2
		Hybrid power assist [%]	4.8	11.0	45.7
		Hybrid battery charging [%]	18.4	21.5	3.1
	SOC window [%]		15.6	7.6	4.6
	Cell current RMS [A]		8.0	5.8	4.0
	Friction brake energy [kJ]		12	71	342
	Regenerative energy [kJ]		1680	1620	1350
	MG1 electrical loss [kJ]		2	16	44
	MG2 electrical loss [kJ]		267	222	220
	ICE averaged BSFC [g/kWh]		205.0	211.1	220.8

HWFET	Operating mode selection	Pure electric [%]	50.5	43.8	38.2
		Series [%]	1.4	2.2	3.4
		Hybrid power assist [%]	0.8	1.2	1.6
		Hybrid battery charging [%]	47.3	52.8	56.8
	SOC window [%]		17.9	16.5	11.1
	Cell current RMS [A]		13.2	10.5	8.6
	Friction brake energy [kJ]		1	5	21
	Regenerative energy [kJ]		421	416	401
	MG1 electrical loss [kJ]		7	10	15
	MG2 electrical loss [kJ]		260	207	175
	ICE averaged BSFC [g/kWh]		205.8	209.3	211.8
US06	Operating mode selection	Pure electric [%]	43.0	30.5	29.4
		Series [%]	10.5	17.6	15.9
		Hybrid power assist [%]	13.9	29.1	38.1
		Hybrid battery charging [%]	32.6	22.8	16.6
	SOC window [%]		11.2	10.9	10.1
	Cell current RMS [A]		15.6	9.8	8.3
	Friction brake energy [kJ]		15	385	551
	Regenerative energy [k]		1707	1338	1172
	MG1 electrical loss [kJ]		29	49	46
	MG2 electrical loss [kJ]		186	178	170
	ICE averaged BSFC [g/kWh]		208.4	211.4	212.0
RWC_uphill	Operating mode selection	Pure electric [%]	43.1	35.6	29.2
		Series [%]	5.6	6.7	9.2
		Hybrid power assist [%]	19.2	22.8	37.9
		Hybrid battery charging [%]	32.1	34.9	23.8
	SOC window [%]		10.4	8.1	7.1
	Cell current RMS [A]		14.5	9.3	7.6
	Friction brake energy [kJ]		147	661	875
	Regenerative energy [kJ]		2283	1769	1555
	MG1 electrical loss [kJ]		18	29	43
	MG2 electrical loss [kJ]		237	212	203
	ICE averaged BSFC [g/kWh]		207.3	210.6	212.8
RWC_downhill	Operating mode selection	Pure electric [%]	73.4	58.6	54.7
		Series [%]	1.8	7.3	7.7
		Hybrid power assist [%]	10.2	33.0	35.9
		Hybrid battery charging [%]	14.6	1.2	1.7
	SOC window [%]		22.0	19.6	17.0
	Cell current RMS [A]		14.4	8.7	7.5
	Friction brake energy [kJ]		367	1257	1557
	Regenerative energy [kJ]		3659	2769	2469
	MG1 electrical loss [kJ]		8	38	41
	MG2 electrical loss [kJ]		363	294	278
	ICE averaged BSFC [g/kWh]		205.7	211.2	213.0

Table 8. Operational statistics for simulated driving missions – Power Split HEV.

Driving mission			Fuel economy only	Battery lifetime of 200 thousand km	Battery lifetime of 300 thousand km
WLTP	Operating mode selection	Pure electric [%]	58.4	41.9	41.7
		Hybrid power assist [%]	14.5	52.5	52.4
		Hybrid battery charging [%]	27.1	5.6	5.9
	SOC window [%]		14.2	8.0	7.7
	Cell current RMS [A]		7.5	4.1	3.9
	Friction brake energy [kJ]		409	575	581
	Regenerative energy [kJ]		1921	1712	1705
	MG1 electrical loss [kJ]		243	263	264
	MG2 electrical loss [kJ]		545	486	484
	ICE averaged BSFC [g/kWh]		202.8	206.7	206.7
NEDC	Operating mode selection	Pure electric [%]	65.8	58.9	58.3
		Hybrid power assist [%]	6.8	9.0	8.9
		Hybrid battery charging [%]	27.4	32.1	32.8
	SOC window [%]		13.8	7.6	7.3
	Cell current RMS [A]		6.3	4.5	4.3
	Friction brake energy [kJ]		211	245	245
	Regenerative energy [kJ]		903	860	860
	MG1 electrical loss [kJ]		102	101	102
	MG2 electrical loss [kJ]		267	253	252
	ICE averaged BSFC [g/kWh]		203.1	205.8	205.5
UDDS	Operating mode selection	Pure electric [%]	72.0	63.1	45.6
		Hybrid power assist [%]	5.3	16.9	52.5
		Hybrid battery charging [%]	22.7	19.9	2.0
	SOC window [%]		12.3	8.7	5.2
	Cell current RMS [A]		7.4	5.8	4.1
	Friction brake energy [kJ]		353	378	495
	Regenerative energy [kJ]		1565	1534	1387
	MG1 electrical loss [kJ]		105	110	118
	MG2 electrical loss [kJ]		377	352	323
	ICE averaged BSFC [g/kWh]		202.9	205.2	211.6
HWFET	Operating mode selection	Pure electric [%]	23.7	15.5	14.6
		Hybrid power assist [%]	34.2	47.3	47.6
		Hybrid battery charging [%]	42.2	37.2	37.8
	SOC window [%]		8.0	4.0	2.9
	Cell current RMS [A]		6.8	4.9	3.9
	Friction brake energy [kJ]		83	103	115
	Regenerative energy [kJ]		396	372	357
	MG1 electrical loss [kJ]		207	219	217
	MG2 electrical loss [kJ]		324	311	308
	ICE averaged BSFC [g/kWh]		203.1	204.0	204.4
US06	Operating mode selection	Pure electric [%]	33.3	28.5	26.0
		Hybrid power assist [%]	48.0	67.4	71.3
		Hybrid battery charging [%]	18.7	4.1	2.7
	SOC window [%]		14.7	10.2	6.4
	Cell current RMS [A]		12.8	7.9	4.2
	Friction brake energy [kJ]		350	723	1148
	Regenerative energy [kJ]		1606	1137	603
	MG1 electrical loss [kJ]		164	172	180
	MG2 electrical loss [kJ]		337	311	284
	ICE averaged BSFC [g/kWh]		202.8	204.5	206.2

RWC_uphill	Operating mode selection	Pure electric [%]	40.7	36.6	28.1
		Hybrid power assist [%]	24.7	37.6	53.6
		Hybrid battery charging [%]	34.6	25.8	18.3
	SOC window [%]		16.9	9.5	3.1
	Cell current RMS [A]		13.9	8.8	2.8
	Friction brake energy [kJ]		594	949	1847
	Regenerative energy [kJ]		2141	1694	564
	MG1 electrical loss [kJ]		209	237	277
	MG2 electrical loss [kJ]		435	398	347
	ICE averaged BSFC [g/kWh]		203.3	205.2	211.2
RWC_downhill	Operating mode selection	Pure electric [%]	68.1	56.5	47.3
		Hybrid power assist [%]	17.2	42.8	52.6
		Hybrid battery charging [%]	14.7	0.7	0.1
	SOC window [%]		22.5	17.1	8.6
	Cell current RMS [A]		13.7	7.8	4.5
	Friction brake energy [kJ]		1130	1931	2715
	Regenerative energy [kJ]		3461	2454	1468
	MG1 electrical loss [kJ]		118	145	166
	MG2 electrical loss [kJ]		470	380	326
	ICE averaged BSFC [g/kWh]		203.0	205.4	207.2